FISEVIER

Contents lists available at ScienceDirect

Resources, Conservation & Recycling

journal homepage: www.elsevier.com/locate/resconrec



Full length article

Concrete with discrete slender elements from mechanically recycled wind turbine blades



Ardavan Yazdanbakhsh^{a,*}, Lawrence C. Bank^b, Klaus-Alexander Rieder^c, Yuan Tian^d, Chen Chen^d

- ^a Department of Civil Engineering, City College of New York, Steinman Hall 110, 160 Convent Avn., New York, NY 10031, USA
- b Department of Civil Engineering, City College of New York, Steinman Hall 103, 160 Convent Avn., New York, NY 10031, USA
- ^c GCP Applied Technologies, 62 Whittemore Ave, Cambridge, MA 02140, USA
- ^d Department of Civil Engineering, City College of New York, Steinman Hall 194, 160 Convent Avn., New York, NY 10031, USA

ARTICLE INFO

Keywords: Concrete GFRP Needles Recycled Wind turbine blade

ABSTRACT

A wind turbine blade shell made of glass fiber reinforced polymer (GFRP) composite materials was mechanically processed into slender elements referred to as "Needles". The Needles were used to replace 5% and 10% of the coarse aggregate, by volume, in concrete mixtures that were tested to investigate a number of important properties of fresh and hardened concrete. It was found that the Needles did not affect the stability and workability of fresh concrete negatively. Although the incorporation of the Needles did not have a notable effect on compressive, tensile, and flexural strength of concrete, it resulted in a significant increase in energy absorption capacity (toughness) from 1.2 J in control specimens up to 33.3 J in those with 10% Needle replacement. A polymer burn-off test revealed that, due to the directions in which the shell was cut, in most of the Needles glass fibers were perpendicular to the Needle axis, and therefore to the tensile stress carried by the Needles. Although the Needles with transversely-aligned fibers improve the mechanical performance of concrete, if the cutting directions of wind blades can be optimized so that in the majority of the Needles the fibers are primarily aligned longitudinally, improvements are expected to be more significant.

1. Introduction

1.1. Motivation

The use of wind energy has been increasing globally with an accelerating rate. Since 1999 the production of wind power has grown 30 times and the annual installation of new wind turbines has grown 10 times greater in the United States, which is currently the 2nd largest producer of wind power after China (Hunt et al., 2016). The rapid growth of the wind energy industry in the last 15 years has led to a commensurate rapid growth in the amount of wind blade waste that will need to be disposed of in the near future.

The components of modern wind turbine blades are mostly made of glass fiber reinforced polymer (GFRP) composite materials. GFRP materials consist of continuous or discrete glass fibers encased in a matrix of resins that have fiber concentrations typically in the range of 12%–60% by volume (Reynolds and Pharaoh, 2010) and inorganic fillers typically in the range of zero to 20% by volume. GFRP materials used in load-bearing members such as wind blades have a high content of continuous fibers (approximately 50%) and contain very low dosages of fillers, if any. The life span of some of the most widely used load-

bearing GFRP products are relatively short. Wind blades are typically designed for a service life of 20 years (Beauson et al., 2014; Hardee, 2012).

Currently, the vast majority of GFRP waste in the US is landfilled. GFRP materials are non-biodegradable and landfill disposal of GFRP is already severely restricted in a number of countries, including Germany and the Netherlands. It is possible that when the currently produced GFRP materials reach the end-of-life stage landfilling regulation in the rest of the world will be stricter. The recently inaugurated U.S. Department of Energy's Institute for Advanced Composite Manufacturing Innovation (IACMI) has a mandate to increase the ability to recycle composite materials with a goal of 80 percent recyclability within the next decade (IACMI, 2016). The analyses of the data provided by the American Wind Energy Association (AWEA) on the annual number of in-service wind turbines, up to 2015 shows that by 2035 wind blade GFRP waste will amount to over 700,000 tonnes (Arias, 2016). Based on the existing growth in wind energy use it was also estimated that by year 2055 the amount of wind blade waste will be over 2.7 million tonnes.

Recycling GFRP is challenging since approximately 75% of GFRP products (including all of those used in wind blades) are made with

E-mail address: ayazdanbakhsh@ccny.cuny.edu (A. Yazdanbakhsh).

^{*} Corresponding author.

thermoset polymers, which do not melt in high temperature. A number of methods for recycling FRP waste have been developed involving chemical and/or thermal processes for reclaiming the fibers, or mechanical processes such as grinding or shredding GFRP into powder or small fragments for use as fillers in the production of new materials (Yazdanbakhsh and Bank, 2014). In addition, GFRP waste can be incinerated (burnt at high temperature) for producing energy or reducing the waste volume. Among the above-mentioned processes mechanical recycling of GFRP is an attractive option as it has the lowest energy demand and does not incorporate chemical processes. The energy required for mechanical recycling is between 0.5% and 5% of that required for chemical recycling and between 0.4% and 16% of the energy used for thermal recycling (pyrolysis) (Job et al., 2016).

A small number of investigators have studied the use of mechanically processed GFRP as a filler in concrete (Asokan et al., 2009; Tittarelli et al., 2010; Tittarelli and Shah, 2013; Yazdanbakhsh and Bank, 2014) and concrete-polymer composite materials (Ribeiro et al., 2015). The problem with traditional mechanical processing (pulverizing or shredding) is that the recycled products are no longer composite materials; they are mostly separate pieces of damaged fibers and resin particles. When used in concrete, the glass fibers become further damaged by the high alkalinity of concrete, and the resin particles that are low in strength and stiffness, reduce the compressive strength of concrete significantly. Cutting GFRP waste into relatively large pieces that are useable in concrete is an attractive potential recycling option for two reasons: (1) cutting a piece of solid material into large pieces rather than grinding or shredding it into powder or small fragments results in generating a smaller surface area and therefore requires less energy, and (2) cut pieces of GFRP are composite materials (fibers embedded in resin), rather than damaged fiber fragments and resin particles, with mechanical properties the same as those of the GFRP before being processed.

Limited research has been conducted on the properties of concrete incorporating slender elements from cut GFRP waste. In a recent study by Yazdanbakhsh et al. (2016), scrap from production of GFRP reinforcing bars (rebars) with different diameters were cut into short cylindrical pieces with aspect ratio of one (Fig. 1), titled FRP-RA, and used in concrete as full and partial (40% by volume) replacement of coarse aggregate. The study found that the full replacement of coarse aggregate with FRP-RA resulted in approximately 20% reduction in compressive strength and splitting tensile strength of concrete, due to the weak bond between FRP-RA particles (particularly the smooth sawcut base surfaces of the cylindrical pieces) and concrete matrix. In an effort to produce recycled elements that can enhance, rather than decrease, the mechanical performance of concrete, GFRP rebar scrap was cut into short rods to be used as discrete slender reinforcing elements in concrete (Yazdanbakhsh et al., 2017). These elements, referred to as FRP-Needles, had a diameter of 6 mm and a length of 100 mm (Fig. 2). Incorporating FRP-Needles in concrete mixtures to replace



Fig. 1. FRP-RA used as a replacement of coarse aggregate in concrete.



Fig. 2. FRP-Needles with a diameter of 6 mm and length of 100 mm.

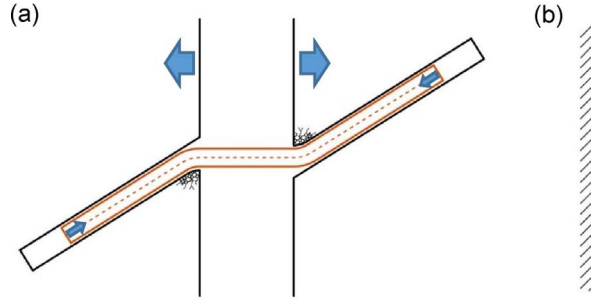
volumetrically 5% and 10% of coarse aggregate (1.76% and 3.52% of concrete) led to 22% and 33% increase in the tensile strength of concrete, respectively. In addition, the use of FRP-Needles in concrete resulted in a significant increase in the post-peak toughness (energy absorption capacity) of concrete. Concrete specimens with 5% and 10% Needle replacement were, respectively 5% and 9% weaker in compression than the control specimens.

1.2. Needles and their fundamental difference from fibers

Fibers, particularly those made from steel and polymers, have been primarily used to control shrinkage cracking in concrete, and also to reduce or even replace rebars in various types of applications such as fiber reinforce concrete (FRC) panels for architectural uses (Bentur and Mindess, 2007), flat structural members such as airport taxiways (Murrell, 1993), slabs-on-ground (Roesler et al., 2006) and elevated slabs (Soranakom et al., 2007). The use of fibers in concrete is attractive since they can be added during mixing to reduce time and labor cost for preparing (bending, cutting and connecting) and placing traditional steel rebars. Rigid FRP fibers have also been studied by (Patnaik et al., 2013, 2014) and (Branston et al., 2016). However, these elements are similar to the fibers used in concrete and do not have the proposed properties and characteristics of Needles.

Fibers have three main shortcomings: (1) They tend to agglomerate and form clumps in fresh concrete. Therefore, the maximum dosage of fiber used in concrete industry is typically limited to 1.0% of the total volume of concrete; (2) Fibers reduce the workability of concrete significantly due to their high specific surface area resulting from their small cross-section dimensions and high aspect ratios. (3) Although fibers can enhance the post-failure toughness of concrete significantly, because only a limited dosage of fibers can be used, their effect on the tensile strength of concrete – an important parameter in the design of structures such as rigid pavements – is typically low (Choi and Yuan, 2005; Nanni, 1988; Wafa and Ashour, 1992), although a number of studies have shown that properly designed FRC can have a higher tensile strength compared to plain concrete (Mobasher 2012). It is expected that Needles, if properly designed, eliminate the aforementioned shortcomings.

When FRC carries increasing external load and a propagating crack intersects a fiber, high tensile strain develops in the fiber in the zone between the crack surfaces, resulting in a high shear stress in the interface between the fiber and cementitious matrix in the zone close to the crack. This shear stress may result in debonding which progresses toward the end of the fiber, after which the fiber will start to move out of its groove at one side of the crack. As shown in Fig. 3a, in order for an inclined fiber (i.e., a fiber that lie at an angle to the crack surface) to slip out, it must bend over crack surfaces. Even fibers made with high-elasticity-modulus materials, such as steel fibers, bend in plastic mode at crack surface during crack opening.



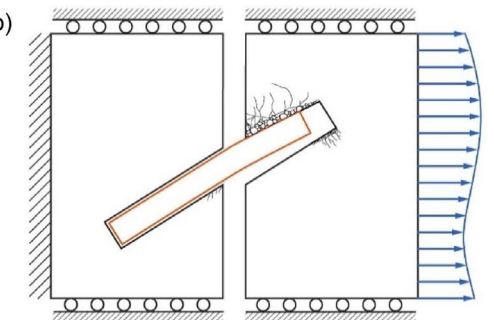


Fig. 3. (a) Fiber pull-out and bending during the growth of a crack in concrete. (b) Local failure and crumbling during opening of a crack bridged by a Needle.

An efficient Needle is very rigid (i.e., has high flexural stiffness) and has high strength in both tension and shear. Therefore, the only way for a concrete crack, which is bridged by such a Needle, to grow in width and is for the concrete encasing the Needle to crumble and/or spall on at least one side of the crack Fig. 3b. Efficient Needles can be produced by selecting materials with high Young's modulus and tensile and shear strengths, and by choosing a large enough Needle cross-section area. Slender elements with large cross-section area (1) have specific surface areas much lower than those of fibers and therefore, do not reduce the workability of fresh concrete significantly; (2) when compared to fibers, constitute a much smaller number of elements per volume; and (3) have high flexural rigidity (EI). Therefore, they are less likely to agglomerate and can be used in high volumetric dosage (Yazdanbakhsh et al., 2017).

2. Experimental program

2.1. Materials

The Needles used in this study were produced from the shell of a wind turbine blade. Wind blade shells are very thick – typically, a few inches – in the regions close to the blade root (where the blade is connected to the rotor) and are fully made of GFRP. The areas of the shell that are further away from the root are thinner, and in low load carrying regions consist of low-density materials such as balsa wood or polymeric foam covered with a very thin layer of glass fiber fabric and resin (i.e., sandwich construction). For the present study, square pieces of a GFRP wind blade shell with a thickness of approximately one inch were used (Fig. 4a). The pieces were provided by the Wind Technology Testing Center (WTTC) of the National Renewable Energy Laboratory (NREL) and were cut off from a wind blade which had been mechanically tested at the center. The information regarding the properties and

the composition of GFRP used for producing the wind blade were confidential and were not made available to the authors. The pieces were curved along two parallel sides of the square and almost flat in the direction of the other two sides (Fig. 4a).

To be able to compare the results of this study with that of the aforementioned previous work by the authors on Needles from GFRP rebars (Yazdanbakhsh et al., 2017) the wind blade Needles were produced to have a similar geometry. For this purpose each of the square pieces was cut into curved rectangles with a short side length of 100 mm (Fig. 4b). The rectangles were subsequently sliced into flat pieces with a width of 100 mm and thickness of 6 mm (Fig. 4c). Grooves with the depth of 2 mm were cut into the surface of half of the flat pieces. Finally, by cutting the flat pieces into slender elements with square cross-sections (6 mm by 6 mm) and length of 100 mm, two types of Needles, namely plain and grooved, were produced (Fig. 5). All the above-mentioned processes were performed by using a table saw with a diamond blade.

For concrete production a mixture of crushed granite and limestone was used as coarse aggregate. The purchased coarse aggregate was regraded in the laboratory using a large sieve shaker to achieve the ASTM No. 56 gradation (nominal maximum size of 25 mm) (ASTM C33, 2013). ASTM graded manufactured (crushed) sand and Type I portland cement were used in all concrete mixes.

2.2. Concrete production, specimen preparation and testing

Five types of concrete mixtures were produced: Control concrete without Needles, concretes with 5% of coarse aggregate replaced volumetrically with plain and grooved Needles, and concretes with 10% of coarse aggregate replaced volumetrically with plain and grooved Needles. Concrete mix proportions are presented in Table 1. In the



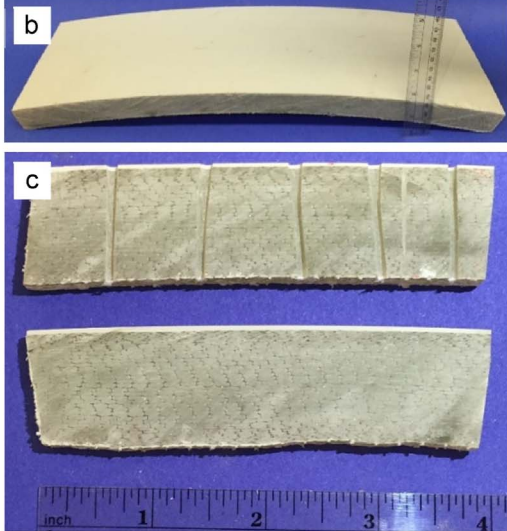


Fig. 4. (a) Square pieces of GFRP shell cut off from a wind blade. In each of these pieces two side are curved (the horizontal sides) and the other two sides are almost flat (b) A rectangular piece of shell with a width of 100 mm cut off from a square piece along the curved side. (c) Flat pieces with a thickness of 6 mm and width of 100 mm cut off from the rectangular pieces.

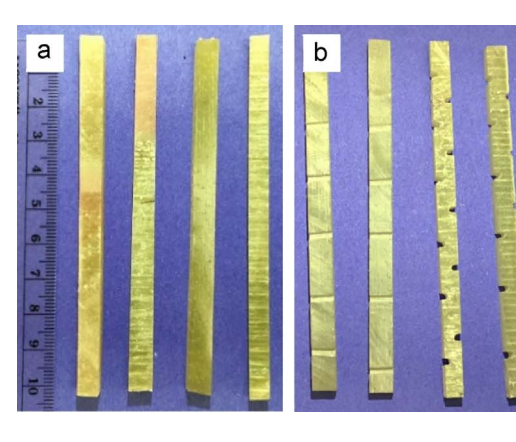




Fig. 5. (a) Plain Needles. (b) Grooved Needles (front and side views). (c) A bucket of plain Needles used in the present study for concrete production.

Table 1Proportions of concrete mixtures (kg per one cubic meter of concrete). SSD is the abbreviation for saturated surface dry.

Mixture	CTRL	PLN-5	PLN-10	GRV-5	GRV-10
Cement	444	444	444	444	444
Water	216	216	216	216	216
Sand (SSD)	632	632	632	632	632
Coarse agg. (SSD)	950	903	855	903	855
Needle	_	34	69	34	69
Needle cont., vol%	-	1.76	3.52	1.76	3.52

mixture notation "CTRL" represents control concrete, and "PLN" and "GRV" represent plain and grooved Needles, respectively. As an example, "GRV-10" represents the concrete mixture in which 10% of coarse aggregate is replaced with grooved Needles. In concrete mixtures that 5% and 10% of coarse aggregate are replaced with Needles the volumetric Needle contents of the concretes are 1.76% and 3.52%, respectively.

Cylinder and beam specimens were produced to test the hardened concrete for compressive strength according to ASTM C39 (2015), compressive modulus of elasticity according to ASTM C469 (2014), splitting tensile strength according to ASTM C496 (2011), and peak (flexural) strength and energy absorption capacity (toughness), according to ASTM C1609 (2012). The cylinders had a diameter of 150 mm and height of 300 mm. The beams were 500 mm long and had a square section with side length of 150 mm. Immediately after removing fresh concrete from the mixer a slump test was performed (ASTM C143, 2015) and the Needle incorporated concretes were visually monitored for signs of segregation or agglomeration of the Needles.

For each of the five concrete mixtures two batches of concrete were produced since with the largest available mixer one batch was not sufficiently large to produce all the required test specimens. The first batch of each mixture was used to produce eight cylinders. Four of the cylinders were used for performing compressive modulus of elasticity tests followed by compressive strength tests and the other four were used for splitting tensile strength tests. The second batch was used to produce three beams used for measuring peak strength and toughness. In addition, from the second batch of each Needle-incorporated mixture one cylinder was cast to be tested for compressive strength. The compressive strength of concrete from both batches of each mixture were compared to detect potential discrepancies in production.

The orientation of the Needles (similar to that of stiff fibers) near mold surfaces is affected by the process of molding, leading to non-random alignments. Some standards of testing FRC beams (ASTM C1609, 2012; ASTM C1399, 2015) require that the dimensions of the mold be at least three times the length of fibers. However, ASTM C1609 allows waiving the "three times fiber length" requirement when longer fibers are used to permit casting specimens with desired dimensions.

All the specimens were tested on the same date; 28 days after casting. The specimens for the modulus of elasticity test were removed one day earlier from the environmental chamber, towel-dried, kept in the laboratory environment for few hours so that their surfaces became dry, and then each instrumented with two wire strain gages mounted circumferentially at diametrically opposite points at the mid-height of the specimen. The average reading of the two strain gages during the compression test were used to calculate the modulus of elasticity according to ASTM C469. The load-displacement responses were recorded during both compressive strength and splitting tensile strength tests.

The beam specimens were tested at the facilities of GCP Applied Technology in Cambridge, MA. Three days before testing, the beams were securely packed, transported from New York to a laboratory at GCP Applied Technology, and immediately immersed in saturated limewater. The setup for measuring the toughness of concrete beams consisted of a third point bending test configuration with a rectangular jig surrounding the specimen and clamped to the beam's lateral surfaces at mid-depth directly over the supports, which form a span of 450 mm (Fig. 6). Two linear variable differential transformers (LVDT) were mounted on the jig at mid-span at both sides of the beam to measure deflection and provide feedback to the actuator of a servo-controlled hydraulic testing machine, thereby constituting a closed-loop displacement-controlled bending test setup that can accurately measure displacement after the peak load. Toughness T_{150}^D was calculated, according to the ASTM C1609, as the area under the load-deflection curve up to the deflection of 3 mm, which is the beam span divided by 150. Equivalent flexural strength ratio $R_{T,150}^D$ was calculated according to the standards prescribed formula:

$$R_{T,150}^{D} = \frac{150 \cdot T_{150}^{D}}{f_{p} \cdot b \cdot d} \cdot 100\% \tag{1}$$



Fig. 6. Closed-loop bending test setup for measuring concrete flexural strength and toughness.

Table 2
Slump test results presented in millimeter.

Batch	CTRL	PLN-5	PLN-10	GRV-5	GRV-10
1 2	125	115	125	115	110
	160	110	110	120	95

where f_p is the peak strength calculated according to $f_p = PL/bd^2$. P and L are the peak load and beam span, respectively. b and d are the average width and depth of the beams, respectively. D is the nominal depth of the beam. In addition, residual strengths f_{600}^D and f_{150}^D at net deflections of L/600 (0.75 mm) and L/150 (3.00 mm) were measured. Since the equivalent flexural strength ratio $R_{T,150}^D$ is the toughness normalized by the peak strength and dimensions of the beam cross-section, this unitless parameter is useful for comparing the results of different studies on concrete reinforced with different types of randomly distributed discrete slender elements performed on beam specimens with different section sizes and peak strength values.

In order to observe the alignment of glass fibers in Needles the resin matrix of a number of the plain Needles were burnt off following the procedure of ASTM D2584 (2011). During the test each Needle specimen is placed on a crucible and is kept in a muffle furnace at $565\,^{\circ}$ C until the polymeric binder fully burns off and disappears.

3. Results and discussion

3.1. Workability and stability of fresh concrete

The slump test results are presented in Table 2, and show that the differences in the slump values of the mixtures, and of the two batches of each mixture, are within the margin of error. The only slump value that stands out among the results is that of the second batch of control mixture, which is 35 mm higher than the slump of the first batch. This difference, although not very significant is possibly due to a minor mismeasurement during the production process. The results in Table 2 show that the slump of GRV-10 mixtures are slightly lower than that of PLN-10 mixtures (on average 15 mm). The difference is due to the higher surface area and rougher surface of the grooved Needles.

The insignificant effect of Needles on concrete workability is a remarkably advantageous characteristic for a discrete reinforcing element. In fiber reinforced concrete high range water-reducing chemical admixtures (superplasticizers) are used to avoid the need to increase the water to cementitious material ratio in concrete. Only a limited dosage of superplasticizers can be used in concrete, beyond which setting time and entrapped air content can increase significantly. Using the allowable dosage to counteract the effect of fibers on workability is a misuse of superplasticizers; when superplasticizers are used in concrete without fibers, less cementitious binder (paste) is required to achieve the desired target compressive strength and workability, and the demand for portland cement can be reduced by 25% (Jeknavorian, 2012), which is a major contribution to the environmental sustainability of concrete

During mixing, removal of concrete from mixers, and casting it was visually observed that the incorporation of Needles did not result in any noticeable segregation of concrete or separation of Needles from the mixtures. The distribution of the Needles in concrete was relatively random and no agglomeration was observed. This finding was further confirmed by observing the fractured surfaces of hardened concrete specimens after mechanical testing. The above-mentioned observations were similar to those from the previous study of the authors on Needles made of GFRP rebars (Yazdanbakhsh et al., 2017).

3.2. Mechanical performance of concrete in compression

The result from measuring the compressive strength and the

Table 3 Results of testing concrete cylinders in compression. f_c and E are the compressive strength and modulus of elasticity of concrete. Subscript m represents the mean values.

		•					
Mixture	Batch- specimen	f_c , MPa	f_{cm} , MPa	Change in f_{cm} , %	E, GPa	E _m , GPa	Change in E_m , %
CTRL	1–1	36.1	36.0	_	24.7	25.9	_
	1–2	36.7			27.4		
	1-3	36.3			23.1		
	1-4	35.0			28.4		
PLN-5	1-1	33.2	35.5	-1.5	29.2	29.1	12.5
	1-2	36.0			28.0		
	1–3	36.0			27.5		
	1–4	36.8			31.8		
	2–1	34.3	34.3	-	-	-	-
PLN-10	1-1	35.6	36.1	0.1	29.2	27.4	5.8
	1-2	35.1			26.8		
	1-3	35.5			27.6		
	1-4	38.1			26.0		
	2–1	35.6	35.6	-	-	-	-
GRV-5	1-1	38.8	38.6	7.2	26.6	27.6	6.3
	1-2	38.9			26.9		
	1–3	37.5			31.6		
	1–4	39.2			25.4		
	2–1	37.2	37.2	-	-	-	-
GRV-10	1-1	34.2	34.4	-4.6	22.6	24.7	-4.7
	1-2	34.6			23.6		
	1-3	35.2			29.1		
	1-4	33.6			23.5		
	2–1	34.7	34.7	-	-	-	-

modulus of elasticity of concrete are presented in Table 3 The average compressive strength of specimens from the first batch of each Needle-incorporated mixture and compressive strength of the single cylinder from the second batch are very close, indicating that the two batches from each mixture have the same compositions and properties.

The results show that the incorporation of both plain and grooved Needles in concrete - particularly the former - has an insignificant impact on the compressive strength of concrete. Replacing 5% and 10% of coarse aggregate with plain Needles resulted in 1.5% reduction and 0.1% increase in the compressive strength of concrete, respectively. Replacing 5% and 10% of coarse aggregate with grooved Needles resulted in 7.2% increase and 4.6% reduction in the compressive strength of concrete, respectively. These changes are within the expected margin of error and do not indicated any beneficial or detrimental impact of the Needles on compressive strength of concrete. According to the authors' previous study (Yazdanbakhsh et al., 2017) the incorporation of Needles from GFRP rebars on compressive strength of concrete was small but clearly negative; 5% and 9% reduction due to the replacement of 5% and 10% of coarse aggregate with Needles. As opposed to the wind blade Needles used in the present study, rebar Needles have a round section without sharp edges (Fig. 2) leading to a weaker bond with cementitious mortar and poor interlock with coarse aggregates.

The test results suggest that the use of Needles, except in the GRV-10 specimens, lead to a small increase in the modulus of elasticity of concrete. The moduli of elasticity of PLN-5, PLN-10 and GRV-5 specimens were 12.5%, 5.8% and 6.3% higher than that of control specimens. The average modulus of elasticity of GRV-10 specimens was 4.7% lower than that of control specimens. The small impact on modulus of elasticity can be contributed to the low volumetric dosage of Needles in concrete (1.76% or 3.52%).

3.3. Mechanical performance of concrete in tension

Test results show that the splitting tensile strength decreases as a result of incorporating Needles in concrete (Table 4). The splitting tensile strength of PLN-5, GRV-5, and GRV-10 specimens were 14%, 13%, and 8% lower than that of the control concrete. The control and

Table 4Results of splitting tensile strength test.

Mixture	Batch-specimen	f_{ct} , MPa	f _{ctm} , MPa	Change in f_{ctm} , %
	-			
CTRL	1–5	2.65	3.35	-
	1–6	3.68		
	1–7	3.46		
	1–8	3.58		
PLN-5	1–5	2.98	2.89	-14
	1–6	3.03		
	1–7	2.77		
	1–8	2.77		
PLN-10	1–5	3.10	3.35	0
	1–6	3.76		
	1–7	3.12		
	1–8	3.43		
GRV-5	1–5	2.93	2.91	-13
	1–6	2.67		
	1–7	3.10		
	1–8	2.94		
GRV-10	1–5	3.12	3.09	-8
	1–6	3.31		
	1–7	3.03		
	1–8	2.90		

PLN-10 specimens had the same average splitting tensile strength. These results are in complete contrast with those from investigating GFRP rebar Needles, which as stated earlier, significantly increased the splitting tensile strength of concrete (22% and 33%, for replacing 5% and 10% of coarse aggregate with Needles, respectively). These findings led to the hypothesis that the tensile strength of wind blade Needles is less than that of rebar Needles. The hypothesis was examined by performing the ASTM D2584 burn-off test on over 10 randomly selected plain Needles.

The results of the burn-off test revealed that in the majority of the Needles glass fibers are aligned transversely – i.e. perpendicular to the Needle axis (Fig. 7a). Only in few of the Needles the majority of the glass fibers were alighted longitudinally – i.e. parallel to the Needle axis (Fig. 7b). In the GFRP rebar Needles studied by the authors (Yazdanbakhsh et al., 2017) all the glass fibers are aligned parallel to

the axis of the Needles (Fig. 7c). The results of the burn-off tests showed that the glass fiber content in wind blade Needles is approximately 73% by weight (57% by volume). The glass content of GFRP rebar Needles is approximately 70% by weight (53% by volume) according to both the test results and the measurements by the manufacturer of the rebars.

Simplified rules of mixture (Bank 2006) and typical mechanical and physical properties of vinyl ester resin and E-glass fibers were used to estimate the mechanical properties of the Needles with longitudinally and transversely aligned glass fibers. The estimated value of the tensile strength of rebar Needles is 1050, which is very close to the average value of 1025 MPa recently reported by the rebar manufacturer from testing 8 rebar specimens in tension. The tensile strength values for wind blade Needles with longitudinally and transversely aligned fibers were estimated to be 1150 MPa and 34 MPa, respectively. In addition, the modulus of elasticity values of the aforementioned Needles were estimated to be 41 GPa and 8 GPa, respectively. The substantial impact of fiber alignment on the mechanical performance of Needles explains the insignificant effect of using wind blade Needles, in which the fibers are predominantly transversely-aligned, on the mechanical performance of concrete. The direction of fibers in different zones of a wind blade shell is selected by designers based on the required structural performance and the geometry of the wind blade. The knowledge of the blade design and the primary direction of fibers in different zones of blade shell can help to select cutting directions that lead to higher numbers of Needles with longitudinally-aligned fibers.

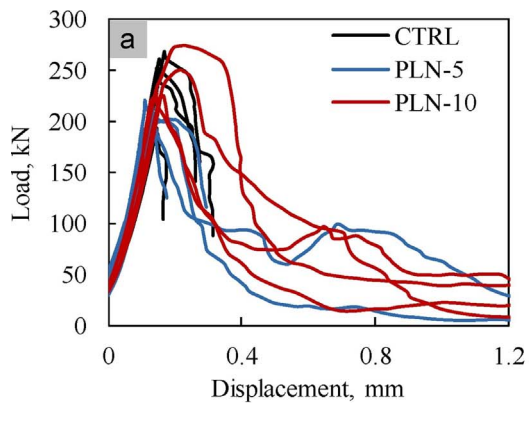
The load-displacement results from splitting tensile strength tests are presented in Fig. 8. The curves were horizontally shifted to account for the initial flexibility of the wooden strips used at the zones of contact between the specimens and testing fixtures. In control specimens the load dropped abruptly after reaching the peak value (Fig. 8). Two of the PLN-5 specimens, and all of the PLN-10 specimens, continued to carry load for deflections beyond 6 mm after the peak load (Fig. 8a). The energy absorption performance of the specimens with grooved Needles was inferior to that of the specimens with plain Needles. Fig. 8b shows that none of the GRV-5 specimens resisted any significant deflection after the peak load. Only one of the GRV-10 specimens continued to carry load beyond the deflection of 6 mm. The reason for the better performance of plain Needles possibly is their higher cross-sectional area; since the grooves are cut off from the surface, the cross section of the Needles in the zones next to the grooves







Fig. 7. Three burnt-off Needles. (a) A wind blade Needle with transversely-aligned fibers. (b) A wind blade Needle with longitudinally-aligned fibers. (c) A GFRP rebar Needle. All the fibers are precisely along the Needle axis.



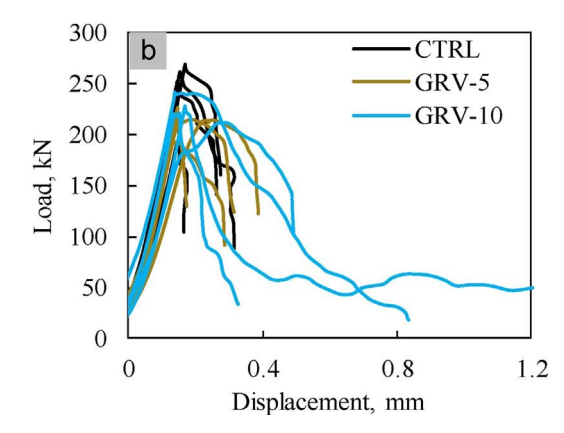


Fig. 8. Load-displacement results from splitting tensile strength testing of concrete specimens with (a) plain and (b) grooved Needles, compared with the results of control specimens.



Fig. 9. A control specimen tested for splitting tensile strength after failure.

are smaller (by 33%) than that of a non-grooved section. Although grooves help to improve the mechanical bond between the Needles and concrete matrix, they generate several weak zones along the axis of the Needles.

Fig. 9 shows a control cylinder specimen after the completion of the splitting tensile strength test, which as expected, was split into two separate pieces. As shown in Figs. 10–13, despite the formation of cracks, none of the Needle-incorporated specimens disintegrated into separate pieces. Fig. 10 shows that all the GRV-5 specimens failed due to the formation and growth of one crack. As can be seen in Figs. 11–13, the majority of the rest of the specimens (GRV-10, PLN-5, and PLN-10) failed due to the formation of more than one crack, indicating a more uniform distribution of stress in concrete. It also can be observed that the lateral expansion (opening) of these specimens, particularly PLN-5 (Fig. 12) and PLN-10 (Fig. 13) are higher than those of GRV-5

specimens, as confirmed by the load displacement results presented in Fig. 8.

3.4. Flexural performance of concrete specimens

The results of the third-point bending test on the beam specimens are presented in Table 5. During testing three of the specimens (two PLN-5 beams and a GRV-5 beam) the servo-controlled hydraulic testing machine stopped abruptly due to a technical problem. Therefore, for those specimens test results are not reported. However, the available results are sufficient to make conclusive assessments of the impact of the Needles on the flexural performance of concrete.

The incorporation of Needles in concrete led to small reductions in the peak strength f_P . The average peak strength decreased from 5 MPa in control specimens to 4.5 MPa in PLN-5 specimens (11% reduction), 4.6 MPa in PLN-10 specimens (9% reduction), and 4.7 MPa in GRV-10 specimens (6% reduction). The average peak strength of GRV-5 specimens was 5.0 MPa (no reduction). The above-mentioned reductions, although slightly less, resemble those from the splitting tensile strength test and similarly can be attributed to the direction of fibers in the Needles.

Fig. 14 shows the fractured surface of a GRV-10 specimen. A small amount of force was required to open the crack that led to failure. Several fractured Needles were observed at the crack surface level. Magnified images of three of those Needles are shown in the Fig. 14. It can be clearly observed that in the fractured Needles fibers are transversely aligned.

The results presented in Table 5 show that replacing 5% and 10% of coarse aggregate by volume with the plain Needles led to the increase of average equivalent flexural strength $R_{7.150m}^{150}$ from 1.1 to 14.0 and 32.3, respectively. When grooved Needles were used the average equivalent flexural strength for 5% and 10% replacements were 12.6 and 24.7, respectively. Table 6 presents selected results from a number of past studies on FRC, with values of equivalent flexural strength, $R_{7.150}^{D}$ for different values of D similar to that of PLN-10 specimens in the present









Fig. 10. GRV-5 specimens tested for splitting tensile strength after failure.

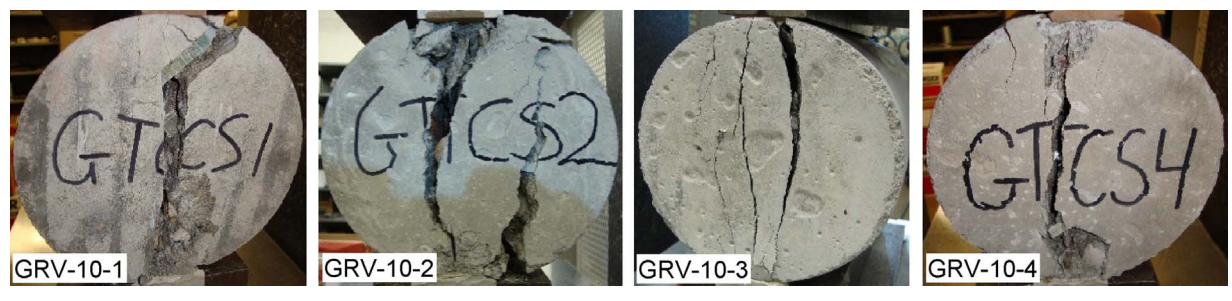


Fig. 11. GRV-10 specimens tested for splitting tensile strength after failure.

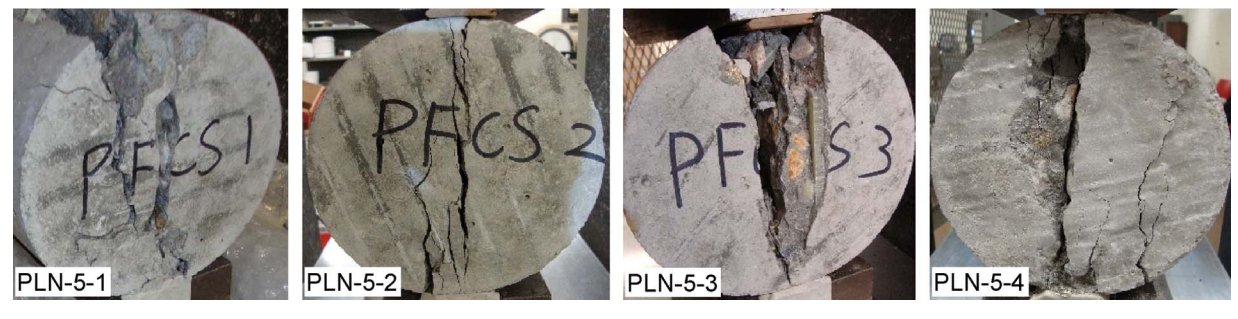


Fig. 12. PLN-5 specimens tested for splitting tensile strength after failure.

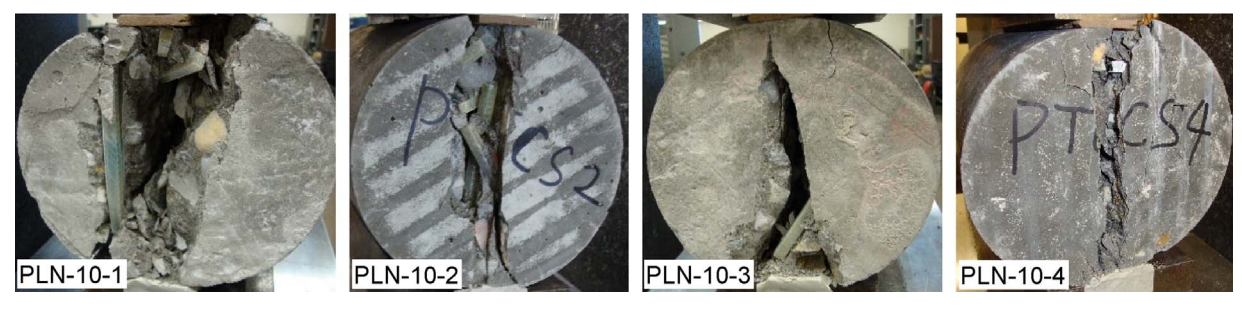


Fig. 13. PLN-10 specimens tested for splitting tensile strength after failure.

Table 5
Results of testing the flexural performance of concrete beams. f_p is the peak strength, f_{600}^{150} and f_{150}^{150} are the residual strength values at net deflections of L/600 and L/150 (0.75 mm, and 3.00 mm), respectively. T_{150}^{150} is the toughness, and $R_{7,150}^{150}$ represents the equivalent flexural strength ratio. Subscript m represents the mean values.

Mixture	Batch-specimen	f_p (MPa)	f_{pm} (MPa)	f_{600}^{150} (MPa)	f_{150}^{150} (MPa)	T_{150}^{150} (J)	T_{150m}^{150} (J)	$R_{T,150}^{150}$	$R_{T,150m}^{150}$
CTRL	2-2	5.1	5.0	0.0	0.0	1.3	1.2	1.2	1.1
	2–3	4.8		0.0	0.0	1.0		1.0	
	2–4	5.2		0.0	0.0	1.4		1.2	
PLN-5	2-2	_	4.5	_	_	_	14.1	_	14.0
	2-3	4.5		1.0	0.0	14.1		14.0	
	2–4	-		-	-	-		-	
PLN-10	2-2	4.7	4.6	2.2	1.1	47.0	33.3	44.6	32.3
	2–3	4.0		1.2	0.6	24.7		27.6	
	2–4	5.1		1.6	0.5	28.3		24.7	
GRV-5	2-2	4.9	5.0	0.6	0.1	11.5	14.3	10.4	12.6
	2–3	-		-	-	-		-	
	2–4	5.2		0.8	0.2	17.1		14.7	
GRV-10	2-2	4.7	4.7	0.8	0.2	16.0	26.3	15.2	24.7
	2-3	4.5		1.6	0.4	26.9		26.8	
	2–4	5.0		1.7	1.0	36.0		32.0	

study. PLN-10 results were selected as benchmark for comparison since they had the highest toughness values. The results presented in the table shows that $R_{T,150}^D$ values similar to that of PLN-10 specimens have been achieved by using (1) steel fibers with volumetric dosages in the

range of 0.2%-1.0%, (2) glass fibers with volumetric dosages in the range of 1.0%-2.0%, and (3) polymeric fibers with volumetric dosages in the range of 0.4%-0.5%. Although these dosages are smaller than the 3.52% Needle content in NDL-10 concrete, the reported increases in

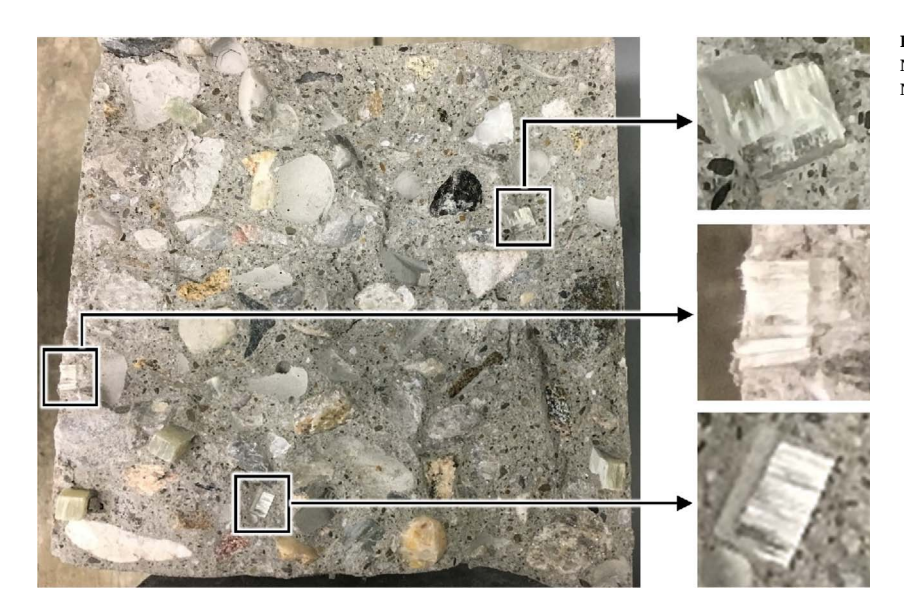
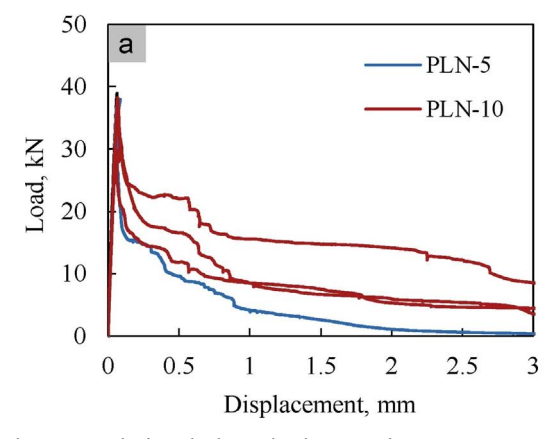


Fig. 14. Fractured surface of a GRV-10 specimen. A number of the Needles have been failed in tension. The magnified views of the failed Needles show that fibers are transversely aligned.

Table 6
Results of a number of past investigations on FRC specimens with equivalent flexural strength values similar to that of PLN-10 specimens in the present study. T_f and E_f are the tensile strength and modulus of elasticity of fibers, respectively. L_f and D_f are the length and nominal diameter of fibers, respectively. D is the beam depth and is equal to the beam width.

Ref.	Fiber material	Fiber shape	T_f	E_f	L_f	L_f/D_f	Content	D	f_c	f_p	T_{150}^{D}	$R_{T,150}^{D}$
			MPa	GPa	mm	-	Vol%	mm	MPa	MPa	J	%
LaHucik et al. (2017)	Modified Olefin	Surface-embossed	640	10	48	67	0.4%	150	57	4.4	36.5	33
	Poly propylene	Surface deformed	550	7	50	75	0.4%	150	48	4.0	30.0	29
	Steel	Hooked	1500	207	60	55	0.2%	150	50	5.1	47.0	37
	High C Steel	Helical	1700	207	25	50	0.4%	150	41	4.2	31.0	29
Bashar et al. (2016)	Steel	Hooked	1100	200	60	80	0.5%	100	32	3.3	6.8	31
	Steel	Hooked	1100	200	60	80	0.8%	100	31	3.8	8.2	32
Liu et al. (2016)	PVA	Straight	1600	39	6	222	0.5%	102	59	6.1	8.6	36
Igbal et al. (2015)	Steel	Hooked	2500	200	13	65	0.5%	100	64	4.4	10.0	34
Tassew and Lubell (2014)	Glass	Straight	2000	76	13	722	2.0%	50	50	7.1	1.7	29
	Glass	Straight	2000	76	19	1056	1.0%	50	51	4.1	1.2	34
Lin et al. (2014)	Steel	Crimped	1100	200	38	33	2.0%	100	85	8.2	17.1	31
Won et al. (2012)	Steel	Hooked	1100	200	30	60	0.7%	100	49	5.0	16.7	30
	Steel	Hooked	1100	200	30	60	1.0%	100	49	5.6	21.7	34



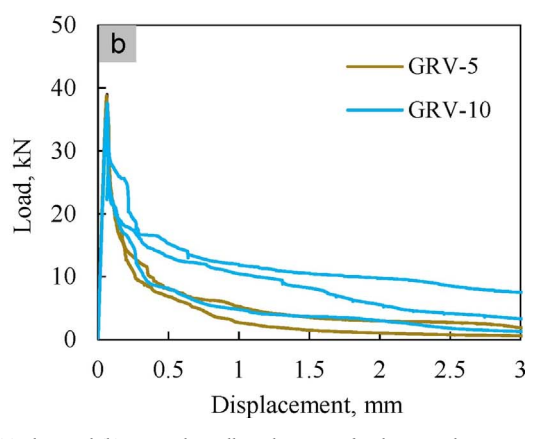


Fig. 15. Load-displacement results from third point bending tests of concrete specimens with (a) plain and (b) grooved Needles. The curves for the control specimens are not shown to avoid congestion. In control specimens, the load drops suddenly and vertically after reaching the peak value.

toughness caused by using Needles are significant considering that in most of the Needles fibers are transversely-aligned. It is expected that if the wind blade shell was cut along the fibers, so that the fibers in all the Needles were longitudinally-aligned, the flexural resistance of the beam specimens would be notably higher.

The load-displacement results of testing the Needle-incorporated concrete beams are presented in Fig. 15. Control beam specimens had no residual strength and therefore the results of testing those specimens

are not shown in the figure. For each type of Needle (plain or grooved), the 10% replacement of coarse aggregate with Needles led to a higher residual strength, compared to 5% replacement. This finding can be confirmed quantitatively by the values of average residual strengths f_{600m}^{150} and f_{150m}^{150} measured at deflections of L/600 and L/150 (Table 5). In PLN-5 and PLN-10 specimens the values of f_{600m}^{150} are 1.0 MPa and 1.7 MPa, respectively, and the values of f_{150m}^{150} are 0.0 MPa and 0.7 MPa, respectively. In GRV-5 and GRV-10 specimens the values of f_{600m}^{150} are



Fig. 16. A Needle in a PLN-5 beam specimen bridging a crack that has grown in width. The concrete surrounding the Needle has crumbled and spalled.

0.7 MPa and 1.4 MPa, respectively, and the values of f_{150m}^{150} are 0.2 MPa and 0.5 MPa, respectively. In addition, the results show that for 10% Needle replacement ratio the residual strength (and therefore toughness) of specimens with plain Needles is higher than that of specimens with grooved Needles.

Fig. 16 shows a plain Needle at the bottom (maximum tension zone) of a PLN-5 beam specimen after the completion of the bending test. The Needle is bridging the crack that led to the beam failure. The image clearly demonstrates that when a crack that is bridged by a Needle grows in width, the concrete matrix surrounding the Needle crumbles and spalls. The Needle shown in the figure did not break in tension, since a relatively short segment of the Needle was at one side of the crack and pulled out from the surrounding matrix. If the Needle was intersected by the crack near its mid-length, it would very likely break during loading – provided the fibers are transversely-aligned – as did the Needles shown in Fig. 14.

4. Conclusions

The findings of the present study show that the Needles produced by cutting a GFRP wind turbine blade shell increased the toughness of concrete significantly despite the fact that fibers were transversely aligned in the Needles. If the wind blade shells can be cut into Needles that primarily constitute longitudinally-aligned fibers, it is expected that the improvement in toughness will be more significant and that the tensile strength of concrete will increase. Prior knowledge of wind blade design or results from performing burn-off tests on samples taken from shells can help to optimize the cutting directions during Needle production. A similar study needs to be performed on wind blade Needles with longitudinally aligned fibers. In addition, the properties of Needles produced from different types of wind blades should be investigated.

Although in GFRP Needles the glass fibers are embedded in and protected by resin, a comprehensive study on durability and long-term performance of concrete incorporating GFRP Needles should be performed. The Needle dimensions in the present study were selected based on concrete specimen size limitations and also for the purpose of comparison with a previous study by the authors on Needles with similar dimensions. A fundamental study needs to be performed to develop models that can determine the optimized dimensions of the Needles based on the properties of the Needle material and the structural application of Needles in concrete.

Acknowledgements

The support of the New York State Energy Research and Development Authority (NYSERDA) under the grant C2CUNY1 by the PowerBridgeNY Program is acknowledged. The authors thank Nathan Post from the Wind Technology Testing Center (WTTC) of the National Renewable Energy Laboratory (NREL), and Larry Trentin from Massachusetts Clean Energy Center for providing a wind blade shell used in the present study. The authors wish to express their gratitude to undergraduate students Jusuf Velovic and Cristian Camilo Alvarez Tuta for processing the wind blade shells into Needles and their contributions to all other experimental phases of the project, and to students Oghosamamwen Agbonlahor, Isabel Zayas, Arelis Fienco and Israel Vilchez for their help during concrete production.

References

ASTM C1399, 2015. Standard Test Method for Obtaining Average Residual-Strength of Fiber-Reinforced Concrete. ASTM International, West Conshohocken, PA, USA.

ASTM C143, 2015. Standard Test Method for Slump of Hydraulic-Cement Concrete. ASTM International, West Conshohocken, PA, USA.

ASTM C1609, 2012. Standard Test Method for Flexural Performance of Fiber-Reinforced Concrete (Using Beam with Third-Point Loading). ASTM International, West Conshohocken. PA. USA.

ASTM C33, 2013. Standard Specification for Concrete Aggregates. ASTM International, West Conshohocken, PA, USA.

ASTM C39, 2015. Standard Test Method for Compressive Strength of Cylindrical Concrete Specimens. ASTM International, West Conshohocken, PA, USA.

ASTM C469, 2014. Standard Test Method for Static Modulus of Elasticity and Poisson's Ratio of Concrete in Compression. ASTM International, West Conshohocken, PA, USA.

ASTM C496, 2011. Standard Test Method for Splitting Tensile Strength of Cylindrical Concrete Specimens. ASTM International, West Conshohocken, PA, USA.

ASTM D2584, 2011. Standard Test Method for Ignition Loss of Cured Reinforced Resins. ASTM International, West Conshohocken, PA, USA.

Arias, F., 2016. Assessment of Present/Future Decommissioned Wind Blade Fiber-Reinforced Composite Material in the United States, Independent Study Report. Supervisor: Lawrence C. Bank. City College of New York.

Asokan, P., Osmani, M., Price, A.D.F., 2009. Assessing the recycling potential of glass fibre reinforced plastic waste in concrete and cement composites. J. Clean. Prod. 17 (9), 821–829.

Bank, L.C., 2006. Composites for Construction. John Wiley & Sons, Hoboken, New Jersey. Bashar, I.I., Alengaram, U.J., Jumaat, M.Z., Islam, A., Santhi, H., Sharmin, A., 2016. Engineering properties and fracture behaviour of high volume palm oil fuel ash based fibre reinforced geopolymer concrete. Constr. Build. Mater. 111, 286–297.

Beauson, J., Lilholt, H., Brøndsted, P., 2014. Recycling solid residues recovered from glass fibre-reinforced composites—a review applied to wind turbine blade materials. J. Reinf. Plast. Compos. 33 (16), 1542–1556.

Bentur, A., Mindess, S., 2007. Fiber Reinforced Cementitious Composites, 2nd ed. Taylor & Francis, New York, NY, 10016.

Branston, J., Das, S., Kenno, S.Y., Taylor, C., 2016. Mechanical behaviour of basalt fibre reinforced concrete. Constr. Build. Mater. 124, 878–886.

Choi, Y., Yuan, R.L., 2005. Experimental relationship between splitting tensile strength and compressive strength of GFRC and PFRC. Cem. Concr. Res. 35 (8), 1587–1591.

Hardee, C., 2012. Improving wind blade manufacturability. Wind Syst. 26–30. Hunt, H., Wanner, C., Hensley, J., 2016. U.S. Wind Industry Annual Market Report – Year Ending 2015. American Wind Energy Association (AWEA), Washington, DC.

IACMI, 2016. Preliminary Technology Roadmap: Phase I. Institute for Advanced Composites Manufacturing Innovations.

Iqbal, S., Ali, A., Holschemacher, K., Bier, T.A., 2015. Mechanical properties of steel fiber reinforced high strength lightweight self-compacting concrete (SHLSCC). Constr. Build. Mater. 98, 325–333.

Jeknavorian, A.A., 2012. Innovations in Chemical Admixture Technology as Related to Sustainability, ACI Spring 2012 Convention. American Concrete Institute, Dallas, TX.

Job, S., Leeke, G., Mativenga, P.T., Oliveux, G., Pickering, S., Shuaib, N.A., 2016. Composite Recycling – Where Are We Now? Composites, UK.

LaHucik, J., Dahal, S., Roesler, J., Amirkhanian, A.N., 2017. Mechanical properties of roller-compacted concrete with macro-fibers. Constr. Build. Mater. 135, 440–446.

Lin, C., Kayali, O., Morozov, E.V., Sharp, D.J., 2014. Influence of fibre type on flexural behaviour of self-compacting fibre reinforced cementitious composites. Cem. Concr. Compos. 51, 27–37.

Liu, X., Zhang, M.-H., Chia, K.S., Yan, J., Liew, J.Y.R., 2016. Mechanical properties of ultra-lightweight cement composite at low temperatures of 0 to $-60\,^{\circ}$ C. Cem. Concr. Compos. 73, 289–298.

Mobasher, B., 2012. Mechanics of Fiber and Textile Reinforced Concrete. CRC Press, Boca Raton, FL.

Murrell, S., 1993. Concrete Airport Pavements Make a Comeback. New York Construction News, McGraw Hill November 29 1993.

Nanni, A., 1988. Splitting-tension test for fiber reinforced concrete. ACI Mater. J. 85 (4).
 Patnaik, A., Miller, L., Adhikari, S., Standal, P., 2013. Basalt FRP minibar reinforced concrete. In: Fiber Concrete. Prague, Czech Republic. pp. 51–52.

Patnaik, A., Miller, L., Standal, P.C., 2014. Fiber reinforced concrete made from basalt FRP minibar. In: Concrete Innovation Conference – CIC 2014. Oslo, Norway, June 11–13.

Reynolds, N., Pharaoh, M., 2010. An introduction to composites recycling. In: Goodship, V. (Ed.), Management, Recycling and Reuse of Waste Composites. Woodhead Publishing, pp. 3–19.

- Ribeiro, M.C.S., Meira-Castro, A.C., Silva, F.G., Santos, J., Meixedo, J.P., Fiúza, A., Dinis, M.L., Alvim, M.R., 2015. Re-use assessment of thermoset composite wastes as aggregate and filler replacement for concrete-polymer composite materials: a case study regarding GFRP pultrusion wastes. Resour. Conserv. Recycl. 104 (Part B), 417–426.
- Roesler, J.R., Altoubat, S.A., Lange, D.A., Rieder, K.-A., Ulreich, G.R., 2006. Effect of synthetic fibers on structural behavior of concrete slabs-on-ground. ACI Mater. J. 103 (1), 3–10.
- Soranakom, C., Mobasher, B., Destrée, X., 2007. Numerical simulation of FRC round panel tests and full-scale elevated slabs. ACI Spec. Publ. 248.
- Tassew, S.T., Lubell, A.S., 2014. Mechanical properties of glass fiber reinforced ceramic concrete. Constr. Build. Mater. 51, 215–224.
- Tittarelli, F., Shah, S.P., 2013. Effect of low dosages of waste GRP dust on fresh and hardened properties of mortars: part 1. Constr. Build. Mater. 47, 1532–1538.
- Tittarelli, F., Kawashima, S., Tregger, N., Moriconi, G., Shah, S.P., 2010. Effect of GRP byproduct addition on plastic and hardened properties of cement mortars. In: 2nd

- International Conference on Sustainable Construction Materials and Technologies.

 June 28, 2010–June 30, 2010. Coventry Business School, Ancona, Italy. pp. 677–687.
- Wafa, F., Ashour, S., 1992. Mechanical properties of high-strength fiber reinforced concrete. ACI Mater. J. 89 (5).
- Won, J.-P., Hong, B.-T., Choi, T.-J., Lee, S.-J., Kang, J.-W., 2012. Flexural behaviour of amorphous micro-steel fibre-reinforced cement composites. Compos. Struct. 94 (4), 1443–1449.
- Yazdanbakhsh, A., Bank, L., 2014. A critical review of research on reuse of mechanically recycled FRP production and end-of-life waste for construction. Polymers 6 (6), 1810–1826
- Yazdanbakhsh, A., Bank, C., Chen, L.C., 2016. Use of recycled FRP reinforcing bar in concrete as coarse aggregate and its impact on the mechanical properties of concrete. Constr. Build. Mater. 121, 278–284.
- Yazdanbakhsh, A., Bank, L.C., Chen, C., Tian, Y., 2017. FRP-Needles as discrete reinforcement in concrete. ASCE J. Mater. Civil Eng. 29 (10), 1–9.